An Improved Solar Spectral Irradiance Composite Record

Thomas N. Woods[1] and Matthew T. DeLand[2]

[1]Laboratory for Atmospheric and Space Physics (LASP), University of Colorado (CU), Boulder, CO, USA

[2]Science Systems and Applications, Inc. (SSAI), Lanham, MD, USA

Corresponding author: Thomas Woods (tom.woods@lasp.colorado.edu)

Submitted to *Earth and Space Science,* March 8, 2021

Key Points:

- A new solar spectral irradiance composite record is available for 1978 to 2020 for the spectral range of 0.5 nm to 1600 nm.
- This Sun-climate record is improved from previous versions with inclusion of the latest solar spectral irradiance measurements.
- Instrument degradation trending and irradiance modeling are part of this development to improve upon solar cycle variability estimates.

Abstract

The solar spectral irradiance (SSI) data set is a key record for studying and understanding the energetics and radiation balance in Earth's environment. Understanding the long-term variations of the SSI over time scales of the 11-year solar activity cycle and longer is critical for many Sun-climate research topics. There are satellite measurements of the SSI since the 1970s that contribute to understanding the solar variability over Solar Cycles (SC) 21 to 24, with most of these SSI measurements in the ultraviolet and only recently in the visible and near infrared for SC-23 and SC-24. A limiting factor for the accuracy of the previous results is the uncertainties for the instrument degradation corrections. Analyses of the past SSI data sets have identified some irradiance offsets and some small residual instrumental trends. These corrections are applied and then combined with a previous SSI composite data set, called the GSFCSSI2 composite, to provide a new SSI composite, called the LASP GSFC SSI #3 (or SSI3). This

improved composite extends the wavelength coverage down to 0.5 nm and up to 1600 nm and the time coverage up to 2020. The solar variability results from the SSI3 are consistent, of course, with the observations from which are used to create the SSI3, but they do differ with some solar variability models, in particular at longer than 900 nm. The development of the SSI3 composite also clarifies the importance of overlapping missions for studying the 11-year solar activity cycle, particularly for wavelengths longer than 200 nm.

Plain Language Summary

The solar radiation is the primary source of energy for Earth. The solar brightness varies on an approximate 11-year cycle, and those solar variations can affect Earth's long-term climate change. To better understand those possible Sun-climate changes, an improved record of the solar spectral irradiance has been developed that merges many individual data sets. These improvements include more accurate information about the solar brightness and variability from the 1978 to 2020 and also extends the previous merged record into the extreme ultraviolet and near infrared regions of the spectrum.

Index Terms: 1650, 7536, 7537, 7538

Keywords: solar spectral irradiance, solar cycle variability

1. Introduction

The solar irradiance is the principle energy input to the global climate system and is critical for studying the radiative energy balance, atmosphere photochemistry, and solar influence on global and regional climate change (e.g., Lean and Rind, 2008). As many solar irradiance observations from a single instrument are shorter than the 11-year solar activity cycle, it is crucial to combine multiple observations into a long-term composite record in order to study how

much solar radiation is deposited in the Earth system on decadal time scales, and thus understand how much energy is available to influence the climate, such as in the cryosphere, atmosphere dynamics, and ocean currents. The total solar irradiance (TSI) is an important observation for studying Earth's net energy balance (e.g., L'Ecuyer et al., 2015), and solar spectral irradiance (SSI) is crucial for understanding where the solar energy is deposited in the Earth system (e.g., Ermolli et al., 2013). In particular, the solar visible and near infrared (NIR) radiation directly heat the surface and oceans, and the solar ultraviolet (UV) heat the atmosphere and drive ozone and other atmospheric photochemistry processes (e.g., Matthes et al., 2016). For example, the response of ozone concentration to the 11-year solar cycle depends strongly on how each wavelength of the SSI varies (Swartz et al., 2012). Significant uncertainty and controversy remain because of the short data records used thus far in model simulations (Haigh et al., 2010; Garcia, 2010). Some of this controversy can be resolved by reducing the uncertainty of solar cycle variations with the latest SSI observations and improving upon the existing SSI composite records.

This research involves updating the latest SSI composite record known as the GSFCSSI2 (DeLand et al., 2019), which in itself is an update of their first SSI composite created by DeLand and Cebula (2008). The GSFCSSI2 composite covers the wavelength range of 120 nm to 500 nm in 1-nm intervals and over the time range from 1978 to 2018. The initial motivation to improve upon this composite record is to extend its spectral coverage into the near infrared (NIR) to 1600 nm and extend it down into the extreme ultraviolet (EUV) to 0.5 nm, so that a more comprehensive coverage of the solar spectrum is represented by the SSI composite. In the process of developing this next version of the SSI composite, that we call the LASP-GSFC SSI #3 (SSI3) composite, additional analysis of the solar cycle variability for the 120-500 nm range was done and incorporated into the new composite record to improve upon trending between different SSI data sets and to fill temporal gaps.

2. Updates for Creating SSI3

There are four significant changes to the GSFCSSI2 composite to create the new SSI3 composite:

1) Revised irradiance levels are established with the latest, more accurate SSI observations,

2) Offsets and trends between different SSI data sets are corrected through comparison of solar variability results from the new SSI observations,

3) SSI composite is extended into the NIR up to 1600 nm, and

4) SSI composite is extended into the EUV down to 0.5 nm.

2.1. **Improvements to GSFCSSI2**

Recent SSI data sets, that utilize updated radiometric calibration facilities, offer improved absolute accuracy relative to many data sets used in creating the GSFCSSI2. Therefore, these new SSI observations provide the most accurate irradiance level to adopt for the SSI3 composite. These updates, as listed in Table 1, are described going from the EUV up through the NIR range.

In the EUV (0.5-120 nm) range, there are the Solar EUV Experiment (SEE) observations between 0.5 nm and 190 nm from the NASA Thermosphere, Ionosphere, Mesosphere, Energetics, and Dynamics (TIMED) mission (Woods et al., 2005) and the EUV Variability Experiment (EVE) observations from 0.5 nm to 122 nm from the NASA Solar Dynamics Observatory (SDO) (Woods et al., 2012). Both of these solar spectral EUV irradiance instruments were calibrated to an accuracy (total uncertainty) of about 5-10% using the Synchrotron Ultraviolet Radiation Facility (SURF) at the National Institute of Standards and Technology (NIST) in Gaithersburg, MD (Woods et al., 2005; Hock et al., 2012). In the far ultraviolet (FUV: 120-200 nm) and middle ultraviolet (MUV: 200-300 nm), the Solar Stellar Irradiance Comparison Experiment (SOLSTICE) aboard the NASA Solar Radiation and Climate Experiment (SORCE) satellite provides the latest and most-accurate irradiance for the FUV and MUV ranges (McClintock et al., 2005). The SORCE SOLSTICE was also calibrated at NIST SURF with an accuracy of about 2-5% (Snow et al., 2005).

In the near ultraviolet (NUV: 300-400 nm), visible (VIS: 400-800 nm), and NIR (800-1600 nm) ranges, the Spectral Irradiance Monitor (SIM) aboard SORCE provide NUV-VIS-NIR observations (Harder et al., 2005) and the Aura Ozone Monitoring Instrument (OMI) provides SSI observations between 265 nm and 500 nm (Marchenko et al., 2019). The SORCE SIM calibrations have about 5% accuracy and are based on characterizations in the LASP calibration facilities and through in-flight comparisons to the Atmospheric Laboratory for Applications and Science (ATLAS) solar reference spectra (Harder et al., 2010). The OMI solar irradiance levels are based on a solar reference spectrum from Thuillier et al. (2004), and the OMI long-term

precision (as opposed to accuracy) is about 0.1-0.2% (Marchenko and DeLand, 2014). The new SIM observations from the Total and Spectral Solar Irradiance Sensor (TSIS-1) mission are considered the most accurate SSI measurements to date with a total uncertainty of about 0.3% (Richard et al., 2020). We therefore use the first-light TSIS-1 SIM spectrum from March 2018 is used as the reference spectrum for the SSI3 for the 500-1600 nm range. These TSIS-1 adjustments from the SORCE SIM SSI levels are less than 1% for wavelengths shorter than 900 nm and can be as large as 5% longer than 900 nm.

The extended wavelength coverage of the SSI3 product means that there are long periods within the overall data record that do not have daily SSI observations in the EUV and VIS-NIR. To compensate, solar variability proxy models of the observations are developed to fill those long gaps. The proxy model results are also used to evaluate time-dependent changes in the GSFCSSI2 product and to provide offset adjustments for the older SSI sets at some wavelengths in order to maintain consistency with the absolute irradiance level of the more recent SSI data sets. We first describe the creation of the proxy models, followed by our analysis of possible drift corrections for the individual SSI data sets.

For accurate proxy modeling, one wants to use an indicator of solar variability for the appropriate solar atmospheric layer for each emission (wavelength) (e.g., Woods et al., 2000). The solar atmospheric layers that have distinct SSI variability characteristics are the photosphere, chromosphere, transition region, and corona. While each layer contributes emissions over many wavelengths, the dominant emissions for each wavelength range are as follows. The photospheric emissions dominate in the NUV-VIS-NIR. The chromosphere emissions begin to play a larger role in the MUV and dominate in the FUV. The two brightest chromospheric emissions are the Ca II emissions near 495 nm and the Mg II emissions near 280 nm. The transition region emissions are dominated by H and He emissions in the EUV and FUV. The emissions from the hot corona are from highly ionized plasma and dominate in the lower EUV and X-ray ranges.

The solar variability proxies considered include well established proxies for those solar layers, with data records that extend back to at least 1980. The 10.7 cm radio flux (F10.7; Tapping, 2013) is primarily generated in the corona. The composite H I Lyman-alpha (Woods et al., 1997; Woods et al., 2000, Machol et al., 2019a) is a transition region emission. The Mg II core-to-wing index (Viereck et al., 2004, Snow et al., 2019) is a chromospheric emission. For

wavelengths shorter than 300 nm where solar active regions dominate the solar variability on short and long time scales, a single proxy can provide reasonable estimates for solar variability. There is a transition in the MUV-NUV range where two proxies are required to adequately estimate the two main components of photospheric solar variability: dark sunspots and bright faculae. The San Fernando Observatory (SFO) solar images of the Sun for the photospheric red (672 nm) continuum and chromospheric Ca II emission are integrated over the solar disk to provide excellent proxies for the dark sunspots and bright faculae, respectively (Chapman et al., 1992; Chapman et al., 2012). Woods et al. (2015) further refines those two photospheric variability indicators by using the total solar irradiance (TSI, being SSI integrated over all wavelengths). The photospheric proxy model is also referred to as the two-component (2C) model.

For each wavelength and in each new data set (OMI, SORCE, TIMED, SDO), a linear regression fit is analyzed using each of the above mentioned proxies. Equation 1 is used for the single proxy model fits, and Equation 2 is used for the 2C proxy model. As the reference data set provides the absolute scale, these equations are parameterized to model just the solar variability (difference from solar cycle minimum conditions). The goodness of fit is examined to determine which proxy is best for each wavelength, which is in bins of 1 nm from the GSFCSSI2 composite. These proxies are summarized in Table 2 along with listing the wavelength ranges for where each proxy is best suited for estimating the solar variability.

The single proxy model is defined as follows:

$$\frac{E-E_{min}}{E_{min}} = C_{ST} \cdot \frac{P-P_{81}}{P_{min}} + C_{LT} \cdot \frac{P_{81}-P_{min}}{P_{min}} \quad (1)$$

where $E(\lambda,t)$ is irradiance at wavelength (λ) and over time (t), $E_{min}(\lambda)$ is the irradiance value at solar cycle minimum (2008-2009), P(t) is proxy time series, $P_{81}(t)$ is the 81-day smoothed proxy time series, P_{min} is the proxy value at solar cycle minimum. The linear regression coefficients, $C_{ST}(\lambda)$and $C_{LT}(\lambda)$, represent the short-term (ST) and long-term (LT) variations as the contrast (slope) of the irradiance variation relative to the proxy variation. The short-term variations are dominated by 27-day solar rotation of the active regions across the solar disk. The long-term variations are dominated by active region evolution (typically lasting about 7 months for each active region) and the number of active regions that wax and wane over the 11-year solar activity cycle. If the proxy and irradiance are from the same solar atmospheric layer, then the C_{ST} and

C_{LT} can have the same value (Woods et al., 2000), and thus the proxy model (Eq. 1) simplifies to a simple linear relationship between the proxy and irradiance. For completeness, the proxy model adopted for filling gaps in the SSI3 nevertheless uses both the ST and LT variability components for the best proxy identified for each wavelength.

The 2C proxy model is defined as follows:

$$\frac{E-E_{min}}{E_{min}} = C_0 + C_F \cdot F + C_S \cdot S \quad (2)$$

where F(t) is the Faculae proxy and S(t) is the Sunspot proxy. The linear regression coefficients, $C_0(\lambda)$, $C_F(\lambda)$ and $C_S(\lambda)$, represent the offset and slopes of the irradiance variation relative to the proxy variation. The Faculae and Sunspot proxies are similar to the 2-components defined in Woods et al. (2015). In this work, the Mg index and TSI are combined to represent the bright faculae variability and dark sunspot variability. The Faculae proxy is the Mg II index scaled into TSI units with the scaling determined by a linear fit of the Mg index to the TSI. The Sunspot proxy is defined as the difference between the TSI and this Faculae proxy. In other words, the addition of the Faculae proxy and the Sunspot proxy is the TSI.

We next present four examples of the proxy model results at selected wavelengths. Figures 1-4 show the linear fit of each model component, as well as comparison between the measurements and the proxy model estimate. The EUV example is at 3.5 nm using TIMED SEE and the coronal F10.7 proxy (Figure 1). The FUV example is for the C II line at 133.5 nm using SORCE SOLSTICE and the transition region LY-A proxy (Figure 2). The MUV example is at 260.5 nm using SORCE SOLSTICE and chromospheric MG proxy (Figure 3). We note that the C_{ST} and C_{LT} values for the EUV, FUV, and MUV examples are similar to each other, as expected. The NIR example for using the two-component photosphere proxies is at 1500 nm using SORCE SIM (Figure 4). This NIR wavelength has out-of-phase variability where the irradiance during solar cycle "maximum" is lower than that at cycle "minimum". This leads to a negative value for the C_F coefficient in this example, instead of being positive as is the normal case for in-phase solar cycle variability. The F10.7, LY-A, and MG proxies provide similar fit quality for the EUV and FUV ranges, so the choice for selecting the best proxy is not very critical to estimate the long-term variations. However, we note that the short-term solar rotation variability is more sensitive to the choice of proxy as related to the radiative transfer effects for the emissions (e.g. center-to-limb variation).

Figure 5 shows the proxy model parameter values as a function of wavelength. The single proxy model method is used for wavelengths shorter than 290 nm, and the ST and LT parameters are shown in Figure 5A. It is a good indication of the appropriate proxy being used for a specific wavelength if the the ST and LT contrast values are very similar to each other (Woods et al., 2000). The 2C proxy model is used for wavelengths longer than 290 nm, and the 2C model parameters are shown in Figure 5B. The sunspot (SS) proxy is itself mostly negative values, so the positive values for the SS parameter indicate that sunspot darkening is important for those wavelengths, being 290-1600 nm. The parameter values for the faculae proxy are positive for wavelengths shorter than 900 nm and are slightly negative for wavelengths longer than 900 nm. This transition from positive values to negative values is the transition where the emissions are in-phase and out-of-phase with the solar cycle activity.

The original formulation of the GSFCSSI2 product brought all individual data sets to a common absolute irradiance level by normalizing to the ATLAS-3 reference spectrum created by Thuillier et al. (2004). Additional small adjustments were made by forcing agreement between 27-day averaged irradiance values at data set transition dates for each wavelength. For the development of the SSI3 composite, the solar variability proxy models are used to identify offsets from the previous data sets used in GSFCSSI2 and bring them into alignment with the irradiance level of the new, more accurate data sets. The average offset corrections are shown in Figure 6 for the different instrument sets in the GSFCSSI2 composite. The offsets for each data set are small, typically being less than 3%, and so the offsets are consistent with calibration accuracies for those data sets. The largest offsets are at wavelengths shorter than 260 nm, and even larger differences are seen at shorter than 140 nm. The estimated uncertainties for the new reference irradiance levels are shown as the dashed lines in Figure 7. With several of the offsets being higher than the reference uncertainties, the updates for GSFCSSI2 to make the new SSI3 composite are important for a more consistent trend over multiple solar cycles.

In addition to examining the data for a systematic offset for each instrument set at each of its wavelengths, the proxy models are also used to check for any long-term drift in the data sets in the GSFCSSI2 composite. Each proxy data set does not show a trend over multiple solar cycles when compared to other proxy time series. We thus assume that a residual trend between an individual SSI data set and calculated SSI values from a proxy model represents uncorrected degradation in the instrument data set. Figure 7 shows the linear trend corrections for each

GSFCSSI2 data set derived using this approach. Note that most trend values fall below the long-term uncertainties of the new reference data sets (SORCE SOLSTICE and OMI). Larger drift correction results are identified for selected data sets and wavelength ranges (NOAA-9 for $\lambda <$ 210 nm, SME for $\lambda < 160$ nm, UARS SUSIM for $\lambda < 150$ nm).

In summary for the updates to the GSFCSSI2 composite, the new SSI3 composite for the 120 nm to 500 nm range has corrections made to the GSFCSSI2 composite for offsets and long-term trends for each instrument set. Most of those corrections are small; that is, they are within instrument uncertainties. Nonetheless, these corrections do improve the overall consistency of variability over the different solar cycles as discussed later. Figure 8 shows examples of the original GSFCSSI2 irradiance time series and the revised SSI3 irradiance time series at selected wavelengths.

2.2. **Extension into NIR**

A significant revision from the GSFCSSI2 composite to the SSI3 composite is the extension of spectral coverage into the NIR and EUV ranges. For the NIR range extension of 500-1600 nm, the SORCE SIM data are used with an adjustment in its absolute scale to match the TSIS-1 SIM reference spectrum in March 2018 (see Section 2.1). The proxy model for filling temporal gaps in the NIR range is also based on the SORCE SIM data. There are several differences between the SORCE SIM solar cycle variability results and some solar variability models, notably the NRLSSI (Lean et al., 1997, 2005; Coddington et al., 2016, 2017) and SATIRE (Fligge, Solanki, and Unruh, 2000; Ball et al., 2014). In particular, -SORCE SIM shows more in-phase solar cycle variability in the NUV and more out-of-phase solar cycle variability in the NIR (Harder et al., 2009; Fontenla et al., 2011; Woods et al., 2018). At the heart of those differences is understanding and validating the SORCE SIM degradation trends. The SORCE SIM degradation trend is based on a two channel design with one channel used daily, and the other channel used about once a month for tracking degradation. However, assumptions about the amount of degradation for the second channel have to be made to obtain irradiance time series from SORCE SIM. Harder et al. (2009), Woods et al. (2015, 2018), and Mauceri et al. (2020) have provided alternative analysis for the SORCE SIM data trends, yielding slightly different results within the SIM stability uncertainties. The Woods et al. (2018) results are

adopted for the SSI3 composite. Comparisons of the SSI3 solar cycle variability results are provided in Section 3.

The new TSIS-1 SIM instrument is experiencing much less degradation than SORCE SIM due to instrument improvements (Richard et al., 2020). TSIS-1 SIM also has three channels, where the third channel is used only once every six months, and this third channel is providing accurate information about how both the primary and secondary TSIS-1 SIM channels are degrading over time and wavelength. Ideally, the proxy model for the NUV-VIS-NIR ranges will be best improved with the TSIS-1 SIM observations. However, solar irradiance variations during 2018-2020 have been very low, so we are not been able to accurately characterize solar cycle variations from TSIS-2 SIM data yet. The new solar cycle 25 activity is starting to pick up in late 2020, and so a future update with TSIS-1 SIM results is planned for the next generation SSI composite (version 4).

2.3. **Extension into EUV**

The extension of the SSI3 data set into the EUV spectral region (0-120 nm) uses observations from TIMED (2002-2020) and SDO (2010-2020). The TIMED SEE spectral EUV observations are from its EUV Grating Spectrograph (EGS; Woods et al., 2005) from 27 nm to 195 nm with 0.4 nm spectral resolution. The EGS observations used in the SSI3 are from 33 nm to 120 nm, including filling the time gaps with proxy model that was fit to the EGS data using the Lyman-alpha proxy. The SDO EVE spectral EUV observations are from its Multiple EUV Grating Spectrographs (MEGS; Woods et al., 2012) from 6 nm to 106 nm with 0.1 nm spectral resolution. The MEGS observations used in the SSI3 are from 6 nm to 33 nm, including filling the time gaps with proxy model results that were fit to the MEGS data using the Lyman-alpha proxy. The EVE MEGS-A channel (6-37 nm) stopped providing valid solar data in May 2014 when a capacitor had a short in the CCD sensor electronics, so there is limited temporal coverage for the MEGS-A observations (2010-2014). The SDO mission is still on-going but with broadband (~4 nm bandpass) measurements below 34 nm and 0.1 nm resolution spectra above 33 nm.

There are very few spectral observations at shorter than 6 nm to use in the SSI3 composite. However, there are several broadband photometer observations available in the X-ray UltraViolet (XUV: 0.5-40 nm) range. For the SSI3 composite, we have chosen to use the Level 4

product from the XUV Photometer System (XPS) aboard both the TIMED and SORCE satellites. The XPS Level 4 product is a model result with 0.1-nm bins using reference spectra combined to match the signals of the XPS photometer with a 0.1-7 nm bandpass. As described in more detail by Woods et al. (2008), the three components of variability represent the quiet-sun (solar cycle minimum), active regions (daily variability), and flares (minute-scale variations). This Level 4 model for the XUV range has recently been updated so that the reference spectra for these three components include observations from SDO EVE for wavelengths longer than 6 nm and from the Miniature X-ray Solar Spectrometer (MinXSS) CubeSat for wavelengths shorter than 2 nm (Woods et al., 2017). A proxy model fit to the TIMED XPS Level 4 product in 1-nm bins is performed using the F10.7 proxy, and those results are used to fill the time gap before the XPS observations began in 2003. The TIMED XPS data was preferred for this proxy model fit because TIMED XPS with its 3% duty cycle has experienced very minor degradation (<1%) over its mission as compared to SORCE XPS with its 70% duty cycle experiencing moderate degradation (a few %).

2.4. **Composite Uncertainties**

The uncertainties for the SSI3 composite are dependent on data source, wavelength, and time. The uncertainties for the composite reference data period (2003-2020) are more straightforward to define as being the uncertainties of those direct observations from SORCE, OMI, TIMED, and SDO. The proxy model results used to fill time gaps include uncertainties from reference data sets, proxy data, and model fit components. Because the different data sources in the GSFCSSI2 composite (120-500 nm) have offset and trend corrections based on proxy models derived with the reference sources, the uncertainties for those different sources have been effectively updated to the level of the proxy model uncertainties. However, the daily variations for those older data sources from the GSFCSSI2 composite still maintain their measurement precision, so users will notice more day-to-day noise in the earlier measurements as compared to the more recent observations. The proxy model wavelength-dependent uncertainties are shown in Figure 9 and are considered representative of the SSI3 composite total uncertainty. This total uncertainty includes the accuracy of the reference data sets (dominant uncertainty), proxy uncertainty, and model fit uncertainty. This model uncertainty is calculated as the standard deviation of the difference between the proxy model prediction and the reference data set.

The SSI3 uncertainty is shown in Figure 9, along with a comparison of the average solar cycle variability of the SSI3 composite data set (discussed in Section 3). We note that the SSI3 total uncertainty is larger than the solar cycle variability at wavelengths longer than 200 nm, which highlights the importance of having overlapping missions in order to accurately study solar cycle variability at $\lambda > 200$nm from multiple data sets. Fortunately, the SORCE and OMI observations have overlapped with the new TSIS-1 observations in the 200-2400 nm range. At wavelengths shorter than 200 nm, non-overlapping missions could provide good results for solar cycle variability with sufficiently accurate long-term characterization.

An additional conclusion concerns the long-term trending feasibility for the SSI3 composite through comparing the solar cycle variability and the model uncertainty. The model uncertainty shown in Figure 9 is a factor of five or more smaller than the solar cycle variability for most wavelengths shorter than 300 nm, so the solar cycle variability results with the SSI3 composite are most accurate for the EUV, FUV, and MUV ranges. The difference between model uncertainty and solar cycle variability decreases to less than a factor of three for most wavelengths longer than 300 nm, which demonstrates the importance of improving upon the observations and proxy models used for those wavelengths longer than 300 nm. The photosphere 2C model and its two proxies are considered an accurate approach for modeling the TSI and photospheric emissions in the SSI, e.g. as used in the three versions of the NRLSSI model. A primary limitation for modeling the solar variability results with the SSI3 composite in the visible and NIR ranges is the quality of the reference data set, SORCE SIM. The measurement precision and limited long-term stability of the original SORCE SIM design with only two channels have affected the uncertainty for the model fits employed to develop the SSI3 composite. The lessons learned from SORCE SIM have led to improvements for TSIS-1 SIM (Richard et al., 2020) and for the Compact SIM (CSIM) cubesat mission (Richard et al., 2019). As noted in Section 2.2, we anticipate making use of these data to improve the SSI3 composite in the future as solar activity increases during solar cycle 25.

3. Solar Variability Results

A key motivation for developing a solar spectral irradiance composite data set is to provide a consistent data set of the SSI variability covering several decades in order to study the long-term variability, and for use in studies of solar influences in Earth's and other planetary environments.

The focus here is on the approximate 11-year solar activity cycle, which is the consequence of the solar 22-year magnetic cycle (e.g., Cliver, 2014). To identify the solar cycle minimum and maximum dates for solar cycles 21 - 24, the Mg II index was smoothed by 405 days (approximately 15 solar rotations, or 13 months) as shown in Figure 10. The solar cycle does not have a fixed 11-year period, and this analysis shows a 9.7-year period for solar cycle 22 (SC22: 1986-1996), a 12.8 year period for SC23 (1996-2009), and a 10.6 year period for SC24 (2009-2019). Different wavelengths can have different dates for their cycle minima and maxima, but generally the dates are within a few months of each other when using 13-month smoothed data.

The solar cycle variability in irradiance units is calculated as the maximum irradiance minus the minimum irradiance. In this analysis, a 405-day average centered on the minimum and maximum dates of each cycle is used for the variability calculation. While the irradiance level may change from one minimum to another, the SSI data at the 2009 minimum are considered more accurate as they include the reference data sets discussed previously and because of the additional analysis conducted for that period for the Whole Heliosphere Interval (WHI) international campaign (e.g., Gibson et al., 2011; Thompson et al., 2011; Woods et al., 2009). Potential SSI changes between minima are likely to be small relative to the minimum-to-maximum solar cycle amplitude for the SSI3 product, as shown in Figure 7. We therefore use the 2009 minimum irradiance to calculate the spectrally dependent SSI solar cycle variability for all four solar cycles. These results are shown in Figure 11. At many wavelengths shorter than 900 nm, the SC-23 variability is the largest, and the SC-24 variability is the smallest. The SC-24 variability is about a factor two smaller than the other solar cycles for $\lambda < 900$ nm. This variability trend over the four solar cycles is similar to that of the Mg II index (see Figure 10) and other solar proxies. We note that the maximum smoothed Mg II index value available for SC-21 may be lower than the actual cycle maximum value because the Mg II index data only began in November 1978. It is also interesting to note that the largest irradiance changes occur in the near ultraviolet (300-400 nm), even though the SSI peaks in magnitude near 500 nm. At wavelengths longer than 900 nm, the cycle variability is out-of-phase (negative), and again it is seen that SC-24 variability magnitude is about a factor of two smaller than the other solar cycles.

The amount of the solar cycle variability integrated into wide spectral bands is shown in Table 3. The total amount of out-of-phase (negative) cycle variability is much smaller than the total amount of in-phase (positive) variability irradiance, so it is the UV and visible bands that

393 are most important for the total cycle variability. The SSI composite does not include all
394 wavelengths, and the far infrared solar irradiance is expected to have small variability like the
395 visible region. In particular, the integrated SSI3 spectra in the 0-1600 nm range is about 150
396 W/m^2 less than the TSI, and an estimate of far infrared variability is about 0.1 W/m^2 if we
397 assume the average solar cycle TSI relative variability of 0.07%. This reduction of the TSI
398 variability for the far infrared region is the last row in Table 3, called the TSI Adjust 0-1600 nm.
399 So we anticipate that the integrated SSI variability should be slightly less than the observed total
400 solar irradiance (TSI) variability. However, Table 3 shows that the integrated solar cycle
401 variability from the SSI3 composite is about 50% of the TSI variability, except for SC-23 where
402 the SSI3 integrated total variability is 65% of the TSI variability. These unexpected differences
403 are discussed in more detail later in this section.

404 The relative cycle variability, defined as the variability in irradiance units divided by the
405 minimum irradiance, is also shown in Figure 11B. The relative variability is largest for the
406 coronal emissions at the shorter wavelengths, reaching more than a factor of two (100%). The
407 variability for the transition region emissions, such as the H continuum near 90 nm, ranges
408 between 10-50%. The chromosphere variability is 3-10% for the FUV range. The photospheric
409 variability dominates for wavelengths longer than 400 nm. The relative variability is about
410 0.07% between 400 nm and 900 nm, which is comparable to TSI relative variability.

411 Figure 12A compares the SSI3 composite in the EUV and FUV ranges, averaged for all four
412 solar cycles, are compared to the predictions from FISM2 (Chamberlin et al., 2020) and
413 NRLSSI3 (Lean et al., 2020). The SSI3 cycle variability and FISM2 variability agree best in the
414 wavelength ranges of 0.5 nm to 35 nm and 115 nm to 160 nm. The differences in the 35 nm to
415 115 nm range are mostly related to FISM2 proxy model development using SDO EVE version 6
416 data and the SSI3 development using the TIMED SEE observations for that EUV range.
417 Similarly for the 160 nm to 190 nm range, the SSI3 composite has been developed using only the
418 latest SORCE SOLSTICE data as its reference set; whereas, FISM2 model uses multiple data
419 sets. The NRLSSI3 predictions agree very well with the SSI3 cycle variability for the full FUV
420 range.

421 The lower cycle variability for the integrated SSI3 composite relative to the TSI variability is
422 a concern because the magnitude of solar cycle irradiance variability for wavelengths longer than
423 1600 nm (not captured in SSI3) is thought to be small. To explore this result in more detail,

Figures 12B and 12C compare the SSI3 variability results are compared to the NRLSSI3 and SATIRE model results. The SSI3 variability results from the four solar cycles are averaged together for this comparison. We apply the same temporal smoothing (405 days) and solar cycle averaging to the NRLSSI3 model estimates. The SATIRE model variability is based on 27-day smoothing for SC-23 (adopted from Woods et al., 2018), so a scaling factor of 0.65 is applied to align the magnitude of SATIRE variability with the SSI3 variability results in the FUV range from 120 nm to 200 nm. The FUV range is used for this scaling factor calculation due to the higher confidence for the SSI3 variability results in the FUV range (see Section 2.4).

The most obvious difference between the SSI3 variability and the variability from the NRLSSI3 and SATIRE models is the wavelength range for which out-of-phase (negative) variability is observed. The SSI3 variability is negative for wavelengths longer than 900 nm and also for a few wavelengths between 400 and 500 nm. In comparison, both the NRLSSI3 and SATIRE models have negative variability only for wavelengths longer than 1300 nm. This out-of-phase variability is expected for the solar NIR irradiance due to the H^- opacity effects (e.g., Harder et al., 2009); however, the wavelength boundary for the transition from in-phase to out-of-phase in the NIR has not been definitively determined. The spectral dependence of the SORCE SIM observations over the full SORCE mission determine this boundary for the SSI3 composite. Analysis of the SORCE SIM data in shorter six-month intervals suggests that the out-of-phase transition could happen between 900 nm and 1600 nm (Woods et al., 2015). Earlier NRLSSI2 version had this boundary near 1600 nm [Coddington et al., 2016]. Nonetheless, the amount of irradiance showing out-of-phase variability for the SSI3 composite is much smaller than the magnitude of its in-phase variability. If the SSI3 variability for the 900-1600 nm range was similar to the NRLSSI3 / SATIRE variability, then the SSI3 in-phase variability listed in Figure 12 could be about 0.8 W/m^2. That higher value is more similar to the TSI variability adjusted to 0-1600 nm range (bottom row in Table 3). SATIRE in-phase estimate than to the NRLSSI3 in-phase estimate. We note that the NRLSSI3 variability and SATIRE variability are higher by 0.10 W/m^2 and 0.24 W/m^2 than the TSI adjusted variability, respectively. The approximate 0.1 W/m^2 difference between NRLSSI3 and SATIRE in-phase variability estimates is primarily due to variability differences in the 300-800 nm range. These comparisons suggest that the integrated SSI variability from the SSI3 composite and the models currently has an uncertainty of about 20% of the TSI variability amount. We are optimistic that the improved

performance of TSIS-1 SIM observations will enable us to resolve these differences once solar cycle 25 activity increases to a level significantly above solar minimum conditions.

4. Summary and Future Plans

The SSI3 composite data set presented in this paper provides improvements for the individual instrument SSI data sets used in the GSFCSSI2 composite data set and also extends the coverage of the SSI composite to cover the wavelength range from 0.5 nm to 1600 nm and over the time period of 1978 to 2020. The SSI3 composite product has 1-nm wavelength bins from 0.5 nm to 749.5 nm and 5-nm bins from 752.5 nm to 1597.5 nm. The improved accuracy of the TSIS-1 SIM solar irradiance measurements is incorporated into the SSI3 composite to provide its reference irradiance levels. As the TSIS-1 SIM data are currently available only during low solar activity, they do not yet provide solar cycle variability results that can benefit the SSI3 composite. Instead, the SORCE SIM and OMI observations provide the most recent solar cycle variability reference data sets for the NUV, visible, and NIR ranges. The reference data sets in the SSI3 composite for the EUV and FUV ranges are from TIMED SEE, SDO EVE, and SORCE SOLSTICE. The wavelength-dependent uncertainty values for these reference data sets represent the dominant term in the overall uncertainty assigned to the SSI3 composite product.

Integrated SSI3 solar cycle irradiance changes over its full wavelength range (0.5-1600 nm) are smaller than expected when compared to TSI changes. We have also compared the spectral dependence of the SSI3 composite solar cycle variability with model estimates to help clarify those results. The FISM2, NRLSSI3, and SATIRE model predictions for solar cycle variability are mostly consistent with the SSI3 composite results in the UV and visible regions, but there are significant differences in the NIR region. The SSI3 composite has out-of-phase (negative) solar cycle variability for wavelengths longer than 900 nm; whereas, the NRLSSI3 and SATIRE models show out-of-phase cycle variability starting at wavelengths longer than 1300 nm. Resolving those differences with SORCE SIM data alone is not likely because different analyses of the SORCE SIM solar variability have suggested the transition to out-of-phase cycle variability begins at different wavelengths between 900 nm and 1600 nm.

Resolving the spectral location of the transition to out-of-phase (negative) solar cycle variability is of highest priority for the solar irradiance community. As mentioned in Sections 2.2

and 3, the new TSIS-1 SIM results are anticipated to help improve the understanding of the solar cycle variability for the NUV-VIS-NIR ranges. These measurements will become more important as solar cycle 25 activity increases during the TSIS-1 mission and will eventually help to improve the next generation (version 4) of the SSI composite. Additionally, the overlap of OMI, SORCE SIM, TSIS-1 SIM, and CSIM observations in 2019 provides a unique opportunity to validate each data set. Results from such validation efforts are in progress, and those results can also help improve the next SSI composite.

While there are plans to extend the SSI observations for the NUV-VIS-NIR ranges for the foreseeable future with the NASA TSIS series, there is grave concern for future SSI observations that cover the EUV-FUV ranges. The full spectral coverage in the FUV range ended when the SORCE mission ended in February 2020, and the EUV observations from TIMED and SDO are at high risk due to the age of those spacecraft and instruments. The NOAA GOES monitoring program for space weather operations does provide monitoring of a few EUV and FUV wavelengths to continue a limited record of solar variability for those ranges (Machol et al., 2019b). The GOES-R series of four satellites have had two satellites launched already, with GOES-16 in operations now. The GOES-R EXIS observations include low-resolution measurements for the 0.1-0.8 nm, 25-34 nm, 117-140 nm, and 278-282 nm ranges. Those spectral bands are used as variability proxies to estimate the solar variability at other EUV wavelengths (Thiemann et al., 2019). In addition, the FISM2 proxy model can be used to estimate the solar variability for observational gaps in time and wavelength for the EUV and FUV ranges.

Acknowledgements and Data

This research is supported by NASA grant 80NSSC18K1303 at the University of Colorado and NASA grant 80HQTR19C0001 at Science Systems and Applications, Inc. We are thankful to the instrument teams for providing their public data products for this study as listed in Tables 1 and 2. The new SSI3 composite data product and the GSFCSSI2 composite data are served from LISIRD at https://lasp.colorado.edu/lisird/data/lasp_gsfc_composite_ssi/. The proxies, parameterization, and related software of the proxy models developed for the SSI3 are available

514 on GoogleDrive at https://drive.google.com/drive/folders/1t0LL-0-qpHyhMFCwRVWNpmK-
515 bs6_5ld4?usp=sharing

516

517 References

518 Ball, W. T., Krivova, N. A., Unruh, Y. C., Haigh, J. D., & Solanki, S. K. (2014). A new
519 SATIRE-S spectral solar irradiance reconstruction for solar cycles 21-23 and its implications
520 for stratospheric ozone. *Journal of Atmospheric Science, 71*(11), 4086-4101.
521 https://doi.org/10.1175/JAS-D-13-0241.1

522 Chamberlin, P. C., Eparvier, F. G., Knoer, V., Leise, H., Pankratz, A., Snow, M., Templeman,
523 B., Thiemann, E. M. B., Woodraska, D. L., & Woods, T. N. (2020). The Flare Irradiance
524 Spectral Model - Version 2 (FISM2). *Space Weather, 18*, 12.
525 https://doi.org/10.1029/2020SW002588

526 Chapman, G. A., Herzog, A. D., Lawrence, J. K., Walton, S. R., Hudson, H. S., & Fisher, B. M.
527 (1992). Precise ground-based solar photometry and variations of total irradiance. *Journal of*
528 *Geophysical Research, 97*(A6), 8211-8219. https://doi.org/10.1029/91JA03018

529 Chapman, G. A., Cookson, A. M., & Preminger, D. G. (2012). Comparison of TSI from SORCE
530 TIM with SFO ground-based photometry. *Solar Physics, 276*(1-2), 35-41.
531 https://doi.org/10.1007/s11207-011-9867-6

532 Cliver, E. W. (2014). The Extended Cycle of Solar Activity and the Sun's 22-Year Magnetic
533 Cycle. *Space Science Reviews, 186*(1-4), 169-189. https://doi.org/10.1007/s11214-014-0093-
534 z

535 Coddington, O., Lean, J. L., Pilewskie, P., Snow, M., & Lindholm, D. (2016). A solar irradiance
536 climate data record. *BAMS, 97*(7), 1265-1282. https://doi.org/10.1175/BAMS-D-14-00265.1

537 Coddington, O., Lean, J., Pilewskie, P., & Woods, T. (2017). Newly Released Climate Data
538 Records of Total and Spectral Solar Irradiance are based on SORCE Observations. *Global*
539 *Space-based Inter-Calibration System Quarterly Newsletter, 11-1*(A2), 3-5.
540 https://repository.library.noaa.gov/view/noaa/17931

541 DeLand, M. T., & Cebula, R. P. (2008). Creation of a composite solar ultraviolet irradiance data
542 set. *Journal of Geophysical Research, 113*(A11), A11103.
543 https://doi.org/10.1029/2008JA013401

DeLand, M. T., Floyd, L. E., Marchenko, S., & Tiruchirapalli, R. (2019). Creation of the GSFCSSI2 Composite Solar Spectral Irradiance Data Set. *Earth and Space Science*, *6*(7), 1284-1298. https://doi.org/10.1029/2019EA000616

Ermolli, I., Matthes, K., Dudok de Wit, T., Krivova, N. A., Tourpali, K., Weber, M., Unruh, Y. C., Gray, L., Langematz, U., Pilewskie, P., Rozanov, E., Schmutz, W., Shapiro, A., Solanki, S. K., & Woods, T. N. (2013). Recent variability of the solar spectral irradiance and its impact on climate modelling. *Atmospheric Chemistry and Physics*, *13*(8), 3945-3977. https://doi.org/10.5194/acp-13-3945-2013

Fligge, M., Solanki, S. K., & Unruh, Y. C. (2000). Modelling irradiance variations from the surface distribution of the solar magnetic field, *Astronomy and Astrophysics*, *353*, 380-388. https://ui.adsabs.harvard.edu/abs/2000A&A...353..380F

Fontenla, J. M., Harder, J., Livingston, W., Snow, M., & Woods, T. (2011). High-resolution solar spectral irradiance from extreme ultraviolet to far infrared. *Journal of Geophysical Research*, *116*(D20), D20108. https://doi.org/10.1029/2011JD016032

Garcia, R. R., (2010). Solar Surprise?. *Nature*, *467*(7316), 668-669. https://doi.org/10.1038/467668a

Gibson, S. E., de Toma, G., Emery, B., Riley, P., Zhao, L., Elsworth, Y., Leamon, R. J., Lei, J., McIntosh, S., Mewaldt, R. A., Thompson, B. J., & Webb, D. (2011). The Whole Heliosphere Interval in the Context of a Long and Structured Solar Minimum: An Overview from Sun to Earth. *Solar Physics*, *27* (1-2), 5-27. https://doi.org/10.1007/s11207-011-9921-4

Haigh, J. D., Winning, A. R., Toumi, R., & Harder, J. W. (2010). An influence of solar spectral variations on radiative forcing of climate. *Nature*, *467*(7613), 696-699. https://doi.org/10.1038/nature09426

Harder, J., Lawrence, G., Fontenla, J., Rottman, G., & Woods, T. (2005). The Spectral Irradiance Monitor: Scientific Requirements, Instrument Design, and Operation Modes. *Solar Physics*, *230*(1-2), 141-167. https://doi.org/10.1007/s11207-005-5007-5

Harder, J. W., Fontenla, J. M., Pilewskie, P., Richard, E. C., & Woods, T. N. (2009). Trends in Solar Spectral Irradiance Variability in the Visible and Infrared. *Geophysical Research Letters*, *36*(7), L07801. https://doi.org/10.1029/2008GL036797

573 Harder, J. W., Thuillier, G., Richard, E. C., Brown, S. W., Lykke, K. R., Snow, M., McClintock,
574 W. E., Fontenla, J. M., Woods, T. N., & Pilewskie, P. (2010). The SORCE SIM Solar
575 Spectrum: Comparison with Recent Observations. *Solar Physics*, *263*(1-2), 3-24.
576 https://doi.org/10.1007s11207-010-9555-y

577 Hock, R. A., Chamberlin, P. C., Woods, T. N., Crotser, D., Eparvier, F. G., Furst, M.,
578 Woodraska, D. L., & Woods, E. C. (2012). EUV Variability Experiment (EVE) Multiple
579 EUV Grating Spectrographs (MEGS) Radiometric Calibrations and Results. *Solar Physics*,
580 *275*(1-2), 145-178. https://doi.org/10.1007/s11207-010-9520-9

581 L'Ecuyer, T. S., Beaudoing, H. K., Rodell, M., Olson, W., Lin, B., Kato, S., Clayson, C. A.,
582 Wood, E., Sheffield, J., Adler, R., Huffman, G., Bosilovich, M., Gu, G., Robertson, F.,
583 Houser, P. R., Chambers, D., Famiglietti, J. S., Fetzer, E., Liu, W. T., Gao, X., Schlosser, C.
584 A., Clark, E., Lettenmaier, D. P., & Hilburn, K. (2015). The Observed State of the Energy
585 Budget in the Early Twenty-First Century. *Journal of Climate*, *28*(21), 8319-8346.
586 https://doi.org/10.1175/JCLI-D-14-00556.1

587 Lean, J. L., & Rind, D. H. (2008). How natural and anthropogenic influences alter global and
588 regional surface temperatures: 1889 to 2006. *Geophysical Research Letters*, *35*(18), L18710.
589 https://doi.org/10.1029/2008GL034864

590 Lean, J. L., Rottman, G. J., Kyle, H. L., Woods, T. N., Hickey, J. R., & Puga, L. C. (1997).
591 Detection and parameterization of variations in solar mid- and near-ultraviolet radiation
592 (200-400nm). *Journal of Geophysical Research*, *102*(D25), 29939-29956.
593 https://doi.org/10.1029/97JD02092

594 Lean, J. L., Rottman, G., Harder, J., & Kopp, G. (2005). SORCE Contributions to New
595 Understanding of Global Change and Solar Variability, *Solar Physics*, *230*(1-2), 27-53.
596 https://doi.org/10.1007/s11207-005-1527-2

597 Lean, J. L., Coddington, O., Marchenko, S. V., Machol, J., DeLand, M. T., & Kopp, G. (2020).
598 Solar Irradiance Variability: Modeling the Measurements. *Earth and Space Science*, *7*(8),
599 e2019EA000645. https://doi.org/10.1029/2019EA000645

600 Machol, J., Snow, M., Woodraska, D., Woods, T., Viereck, R., & Coddington, O. (2019a). An
601 improved Lyman-alpha composite. *Earth and Space Science*, *6*(12), 2263-2272.
602 https://doi.org/10.1029/2019EA000648

603 Machol, J. L., Eparvier, F. G., Viereck, R. A., Woodraska, D. L., Snow, M., Thiemann, E.,
604 Woods, T. N., McClintock, W. E., Mueller, S., Eden Jr., T. D., Meisner, R., Codrescu, S.,
605 Bouwer, S. D., & Reinard, A. A. (2019b). GOES-R Series Solar X-ray and Ultraviolet
606 Irradiance, in *The GOES-R Series: A New Generation of Geostationary Environmental*
607 *Satellites*, ed. S. J. Goodman, J. Daniels, T. J. Schmit, and R. J. Redmon, Elsevier,
608 Cambridge, MA, Chapter 19, pp. 233-242.

609 Marchenko, S. V., & DeLand, M. T. (2014). Solar spectral irradiance changes during Cycle 24.
610 *The Astrophysical Journal, 789*(2), 117. https://doi.org/10.1088/0004-637X/789/2/117

611 Marchenko, S. V., DeLand, M. T., & Lean, J. L. (2016). Solar spectral irradiance variability in
612 Cycle 24: Observations and models. *Journal of Space Weather and Space Climate, 6*, A40.
613 https://doi.org/10.1051/swsc/2016036

614 Marchenko, S. V., Woods, T. N., DeLand, M. T., Mauceri, S., Pilewskie, P., & Haberreiter, M.
615 (2019). Improved Aura/OMI solar spectral irradiance: Comparisons with independent
616 datasets and model predictions. *Earth and Space Science, 6*(12), 2379-2396.
617 https://doi.org/10.1029/2019EA000624

618 Matthes, K., Funke, B., Andersson, M. E., Barnard, L., Beer, J., Charbonneau, P., Clilverd, M.
619 A., Dudok de Wit, T., Haberreiter, M., Hendry, A., Jackman, C. H., Dretzschmar, M.,
620 Kruschke, T., Kunze, M., Langematz, U., Marsh, D. R., Maycock, A., Misios, S., Rodger, C.
621 J., Schaife, A. A., Seppälä, A., Shangguan, M., Sinnhuber, M., Tourpali, K., Usoskin, I., van
622 de Kamp, M., Verronen, P. T., & Versick, S. (2016). Solar Forcing for CMIP6 (v3.1).
623 *Geoscientific Model Development Discuss*. https://doi.org/10.5194/gmd-2016-91

624 Mauceri, S., Pilewskie, P., Woods, T., Beland, S., & Richard, E. (2020). Intercomparing Solar
625 Spectral Irradiance from SORCE SIM. *Earth and Space Science*, *7*(4). e2019EA001002.
626 https://doi.org/10.1029/2019EA001002

627 McClintock, W. E., Rottman, G. J., & Woods, T. N. (2005). Solar Stellar Irradiance Comparison
628 Experiment II (SOLSTICE II): Instrument Concept and Design. *Solar Physics*, *230*(1-2),
629 225-258. https://doi.org/10.1007/s11207-005-7432-x

630 Richard, E., and the CSIM team. (2019). Compact spectral irradiance monitor flight
631 demonstration mission, *SPIE Proceedings*, 11131, id. 1113105.
632 https://doi.org/10.1117/12.2531268

Richard, E., Harber, D., Coddington, O., Drake, G., Rutkowski, J., Triplett, M., Pilewskie, P., & Woods, T. (2020). SI-traceable Spectral Irradiance Radiometric Characterization and Absolute Calibration of the TSIS-1 Spectral Irradiance Monitor (SIM). *Remote Sensing*, *12*(11), 1818. https://doi.org/10.3390/rs12111818

Snow, M., McClintock, W. E., Woods, T. N., White, O. R., Harder, J. W., & Rottman, G. (2005). The Mg II index from SORCE. *Solar Physics*, *230*(1-2), 325-344. https://doi.org/10.1007/s11207-005-6879-0

Snow, M., Machol, J., Viereck, R., Woods, T., Weber, M., Woodraska, D., & Elliott, J. (2019). A Revised Magnesium II Core-to-Wing Ratio from SORCE SOLSTICE. *Earth and Space Science*, *6*(11), 2106-2114. https://doi.org/10.1029/2019EA000652

Swartz, W. H., Stolarski, R. S., Oman, L. D., Fleming, E. L., & Jackman, C. H. (2012). Middle atmosphere response to difference descriptions of the 11-yr solar cycle in spectral irradiance in a chemistry-climate model. *Atmospheric Chemistry and Physics*, *12*(13), 5937-5948. https://doi.org/10.5194/acp-12-5937-2012

Tapping, K. F. (2013). The 10.7 cm solar radio flux (F10.7). *Space Weather*, *11*(7), 394-406. https://doi.org/10.1002/swe.20064

Thiemann, E. M. B., Eparvier, F. G., Woodraska, D., Chamberlin, P. C., Machol, J., Eden, T., Jones, A. R., Meisner, R., Mueller, S., Snow, M., Viereck, R., & Woods, T. N. (2019). The GOES-R EUVS Model for EUV Irradiance Variability. *Journal of Space Weather and Space Climate*, *9*, A43. https://doi.org/10.1051/swsc/2019041

Thompson, B. J., Gibson, S. E., Schroeder, P. C., Webb, D. F., Arge, C. N., Bisi, M. M., de Toma, G., Emery, B. A., Galvin, A. B., Haber, D. A., Jackson, B. V., Jensen, E. A., Leamon, R. J., Lei, J., Manoharan, P. K., Mays, M. L., McIntosh, P. S., Petrie, G. J. D., Plunkett, S. P., Qian, L., Riley, P., Suess, S. T., Tokumaru, M., Welsch, B. T., & Woods, T. N. (2011). A Snapshot of the Sun Near Solar Minimum: The Whole Heliosphere Interval. *Solar Physics*, *274*(1-2), 29-56. https://doi.org/10.1007/s11207-011-9891-6

Thuillier, G., Floyd, L., Woods, T. N., Cebula, R., Hilsenrath, E., Hersé, M., & Labs, D. (2004). Solar irradiance reference spectra for two solar active levels. *Advances in Space Research*, *34*(2), 256-261. https://doi.org/10.1016/j.asr.2002.12.004

Viereck, R. A., Floyd, L. E., Crane, P. C., Woods, T. N., Knapp, B. G., Rottman, G., Weber, M., Puga, L. C., & DeLand, M. T. (2004). A composite Mg II index spanning from 1978 to 2003. *Space Weather*, *2*(10), 10005. https://doi.org/10.1029/2004SW000084

Woods, T. N., & Rottman, G. J. (1997). Solar Lyman-alpha irradiance measurements during two solar cycles. *Journal of Geophysical Research: Atmospheres*, *102*(D7), 8769-8780. https://doi.org/10.1029/96jD03983

Woods, T. N., Tobiska, W. K., Rottman, G. J., & Worden, J. R. (2000). Improved solar Lyman α irradiance modeling from 1947 through 1999 based on UARS observations. *Journal of Geophysical Research*, *105*(A12), 27195-27216. https://doi.org/10.1029/2000JA00051

Woods, T. N., Eparvier, F. G., Bailey, S. M., Chamberlin, P. C., Lean, J., Rottman, J. G., Solomon, S. C., Tobiska, W. K., & Woodraska, D. L. (2005). The Solar EUV Experiment (SEE): Mission overview and first results. *Journal of Geophysical Research*, *110*(A1), A01312. https://doi.org/10.1029/2004JA010765

Woods, T. N., Chamberlin, P. C., Peterson, W. K., Meier, R. R., Richards, P. G., Strickland, D. J., Lu, G., Qian, L., Solomon, S. C., Iijima, B. A., Mannucci, A. J., & Tsurutani, B. T. (2008). XUV Photometer System (XPS): Improved irradiance algorithm using CHIANTI spectral models. *Solar Physics*, *250*(2), 235-267. https://doi.org/10.1007/s11207-008-9196-6

Woods, T. N., Chamberlin, P. C., Harder, J. W., Hock, R. A., Snow, M., Eparvier, F. G., Fontenla, J., McClintock, W. E., & Richard, E. C. (2009). Solar Irradiance Reference Spectra (SIRS) for the 2008 Whole Heliosphere Interval (WHI). *Geophysical Research Letters*, *36*(1), L01101. https://doi.org/10.1029/2008GL036373

Woods, T. N., Eparvier, F. G., Hock, R., Jones, A. R., Woodraska, D., Judge, D., Didkovsky, L., Lean, J., Mariska, J., Warren, H., McMullin, D., Chamberlin, P., Berthiaume, G., Bailey, S., Fuller-Rowell, T., Sojka, J., Tobiska, W. K., & Viereck, R. (2012). The EUV Variability Experiment (EVE) on the Solar Dynamics Observatory (SDO): Overview of Science Objectives, Instrument Design, Data Products, and Model Developments. *Solar Physics*, *275*(1-2), 115-143. https://doi.org/10.1007/s11207-009-9487-6

Woods, T. N., Snow, M., Harder, J., Chapman, G., & Cookson, A. (2015). A different view of solar spectral irradiance variations: Modeling total energy of six-month intervals. *Solar Physics*, *290*(10), 2649-2676. https://doi.org/10.1007/s11207-015-0766-0

692 Woods, T. N., Caspi, A., Chamberlin, P. C., Jones, A., Kohnert, R., Mason, J. P., Moore, C. S.,
693 Palo, S., Rouleau, C., Solomon, S. C., Machol, J., & Viereck, R. (2017). New Solar
694 Irradiance Measurements from the Miniature X-ray Solar Spectrometer CubeSat. *The*
695 *Astrophysical Journal, 835*(2), 122. https://doi.org/10.3847/1538-4357/835/2/122
696 Woods, T. N., Eparvier, F. G., Harder, J., & Snow, M. (2018). Decoupling solar variability and
697 instrument trends using the Multiple Same-Irradiance-Level (MuSIL) Analysis Technique.
698 *Solar Physics, 293*(5), 76-96. https://doi.org/10.1007/s11207-018-1294-5
699
700

Table 1. Observations used in the new SSI3 composite record.

The SSI3 composite includes updates to the GSFCSSI2 composite and additions using data from the following instruments.

Instrument	Wavelength Range in SSI3	Spectral Resolution	Time Range	Data Reference [with those licenses, and these access restrictions if any].
GSFCSSI2 Composite (SBUV, SME, UARS, SORCE, OMI)	120-500 nm	1.0 nm	1978-2018	DeLand et al., 2019
TSIS-1/SIM	500-1600 nm	1-10 nm	Mar. 14, 2018 Ref. Spectrum	Richard et al., 2020
SORCE/SIM	500-1600 nm	1-10 nm	2003-2020	Harder et al., 2005
Aura/OMI	265-500 nm	0.5 nm	2004-2020	Marchenko et al., 2019
SORCE/SOLSTICE	120-265 nm	0.1 nm	2003-2020	McClintock et al., 2005
TIMED/SEE	0.5-6, 33-120 nm	0.4-1 nm	2002-2020	Woods et al., 2005
SDO/EVE	6-33 nm	0.1-1 nm	2010-2020	Woods et al., 2012

Table 2. Solar Variability Proxy Model Choices.

Temporal gaps between measured SSI data are filled with solar variability proxy model estimates.

Solar Proxy (solar atmos. Layer)	Wavelength Range in SSI3	Reference Instrument for Proxy Model	Proxy Reference [with those licenses, and these access restrictions if any].
F10.7 (corona)	0.5 – 6 nm	SORCE/XPS	Tapping, 2013
H I Lyman-alpha (transition region)	6 – 33 nm 33 – 120 nm 120 – 208 nm	SDO/EVE TIMED/SEE SORCE/SOLSTICE	Woods et al., 2000 Machol et al., 2019a
Mg II C/W Index (chromosphere)	208 – 290 nm	SORCE/SOLSTICE	Viereck et al., 2004 Snow et al., 2019
Dark Sunspots & Bright Faculae (photosphere, 2C)	290 - 500 nm 500 - 1600 nm	Aura/OMI SORCE/SIM	Chapman et al., 1992, 2012 Woods et al., 2015

Table 3. Solar Cycle Variability Results in Broad Bands.

Variability is in units of W/m^2. TSI variability results are from Woods et al. (2018) TSI composite.

Wavelength Band	SC-21 (1981)	SC-22 (1991)	SC-23 (2002)	SC-24 (2014)
0-250 nm	0.052	0.051	0.053	0.027
250-500 nm	0.307	0.277	0.485	0.229
500-900 nm	0.257	0.194	0.295	0.114
900-1600 nm	-0.117	-0.131	-0.093	-0.066
SSI3 0-1600 nm	**0.499**	**0.392**	**0.740**	**0.303**
TSI Variability	1.058	0.888	1.134	0.725
TSI Adjust 0-1600 nm	0.942	0.791	1.009	0.646

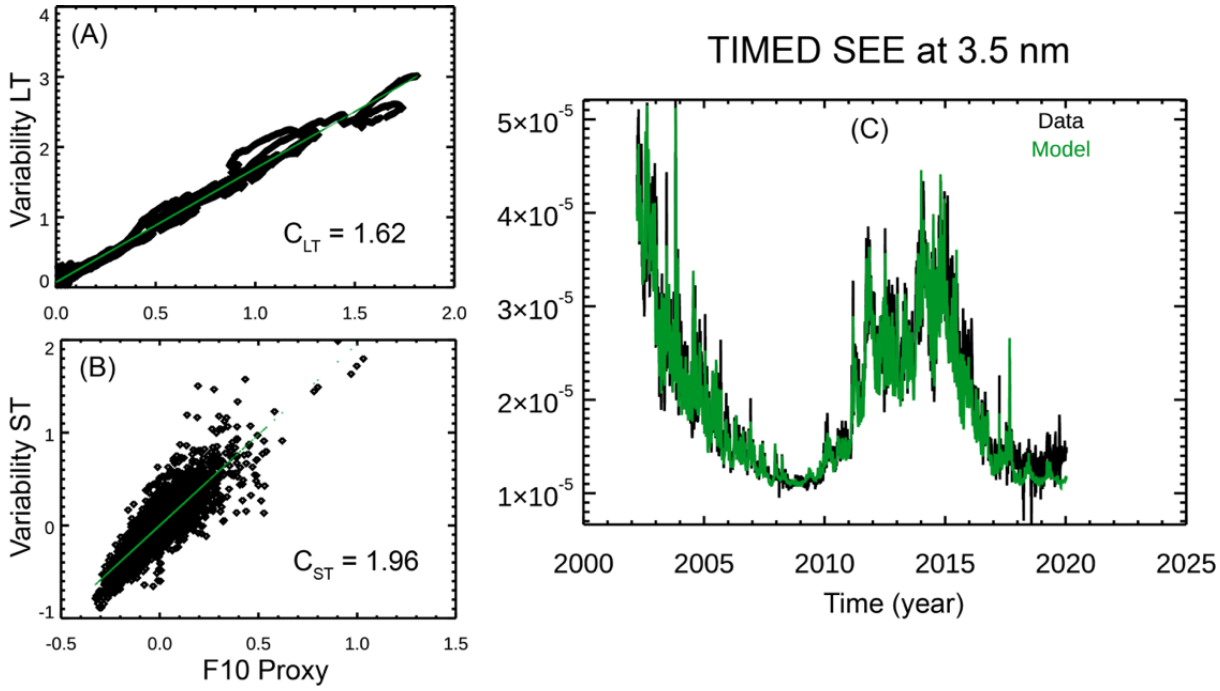

Figure 1. Proxy model fit of TIMED SEE data at 3.5 nm using the F10 proxy is shown for LT variability (panel A), ST variability (panel B), and comparison of data and model (panel C). The variability components shown in panels A and B are unitless (see Equation 1), and the irradiance in panel C has units of $W/m^2/nm$. The average relative difference between data and model irradiance is 15%. The ratio of this 15% to the solar cycle relative variability of 300% at 3.5 nm is 5%, thus indicating a very strong correlation for the solar cycle variability.

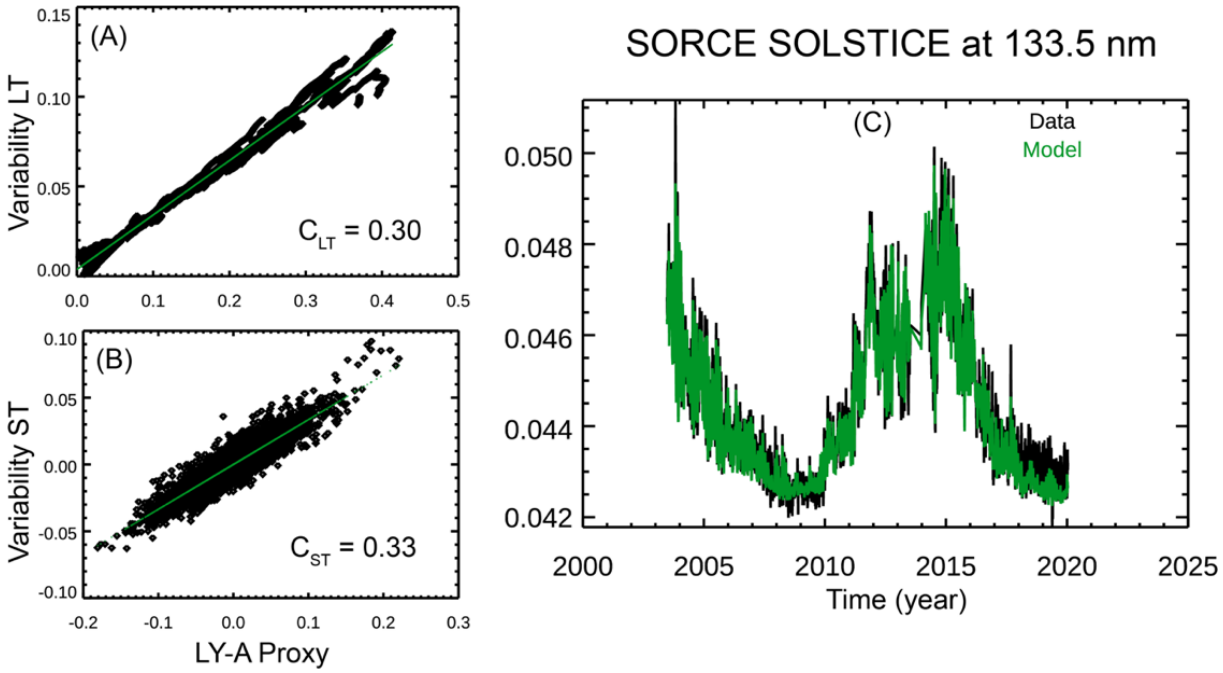

Figure 2. Proxy model fit of SORCE SOLSTICE data at 133.5 nm using the LYA proxy is shown for LT variability (panel A), ST variability (panel B), and comparison of data and model (panel C). The average relative difference between data and model irradiance is 0.8%. The ratio of this 0.8% to the solar cycle relative variability of 14% at 133.5 nm is 6%, indicating a very strong correlation for the solar cycle variability. SORCE has an observational gap in the second half of 2013.

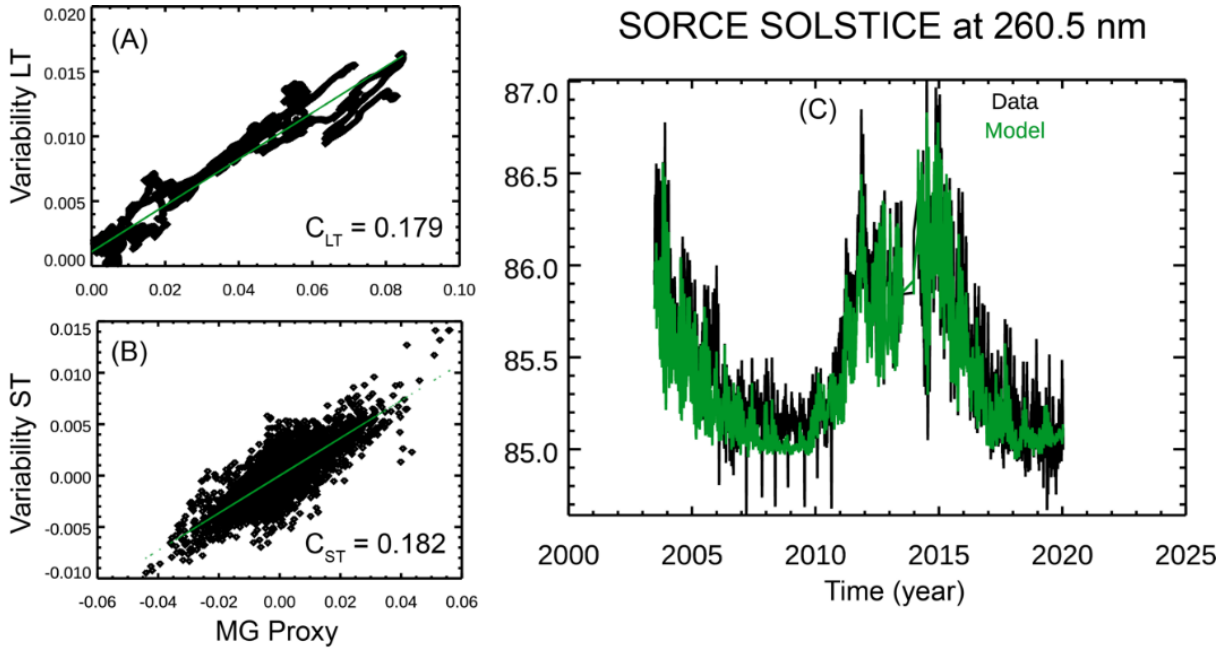

Figure 3. Proxy model fit of SORCE SOLSTICE data at 260.5 nm using the MG proxy is shown for LT variability (panel A), ST variability (panel B), and comparison of data and model (panel C). The average relative difference between data and model irradiance is 0.2%. The ratio of this 0.2% to the solar cycle relative variability of 1.8% at 260.5 nm is 11%, thus indicating a strong correlation for the solar cycle variability. SORCE has an observational gap in the second half of 2013.

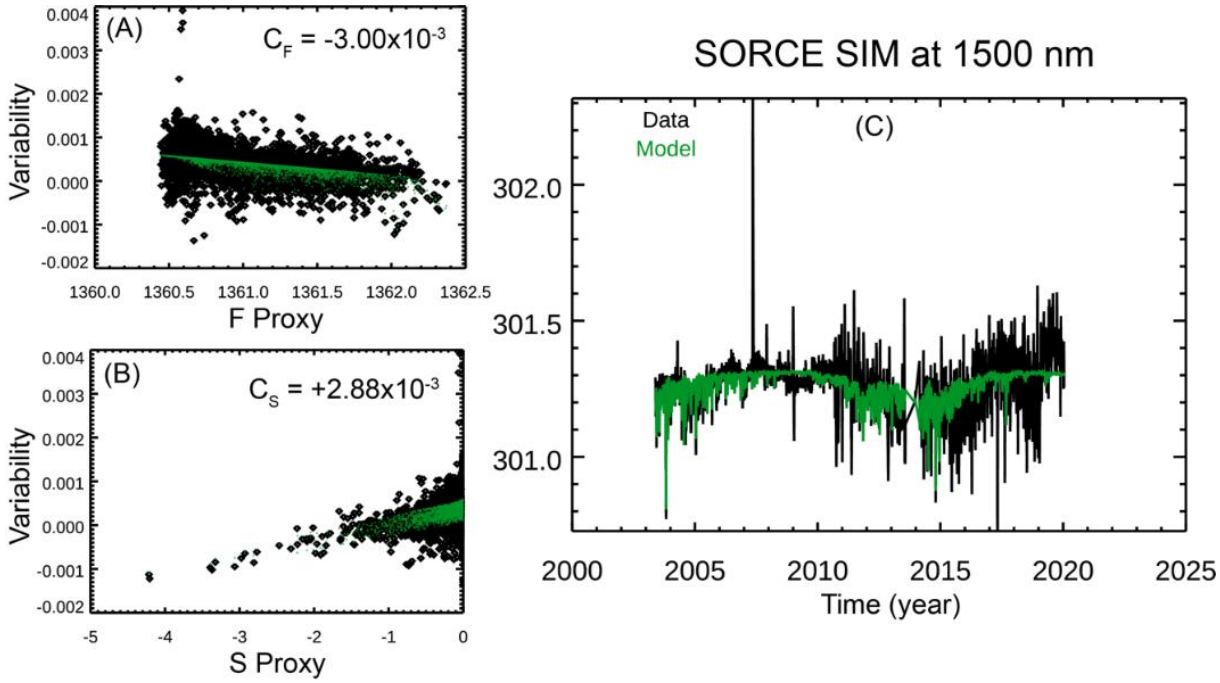

Figure 4. Proxy model fit of SORCE SIM data at 1500 nm using the 2-Component photosphere proxies is shown for Faculae (F) proxy variability (panel A), Sunspot (S) proxy variability (panel B), and comparison of data and model (panel C). This wavelength, as well as most other NIR wavelengths, has out-of-phase variability for the 11-year solar cycle. The average relative difference between data and model irradiance is 0.03%. The ratio of this 0.03% to the solar cycle relative variability of -0.07% at 1500 nm is 43%, thus indicating a moderate correlation for the solar cycle variability. These larger differences are primarily due to the decreased quality (more noise) of the SIM data after 2011, which is caused by having to power cycle SIM every orbit due to SORCE's low battery capacity.

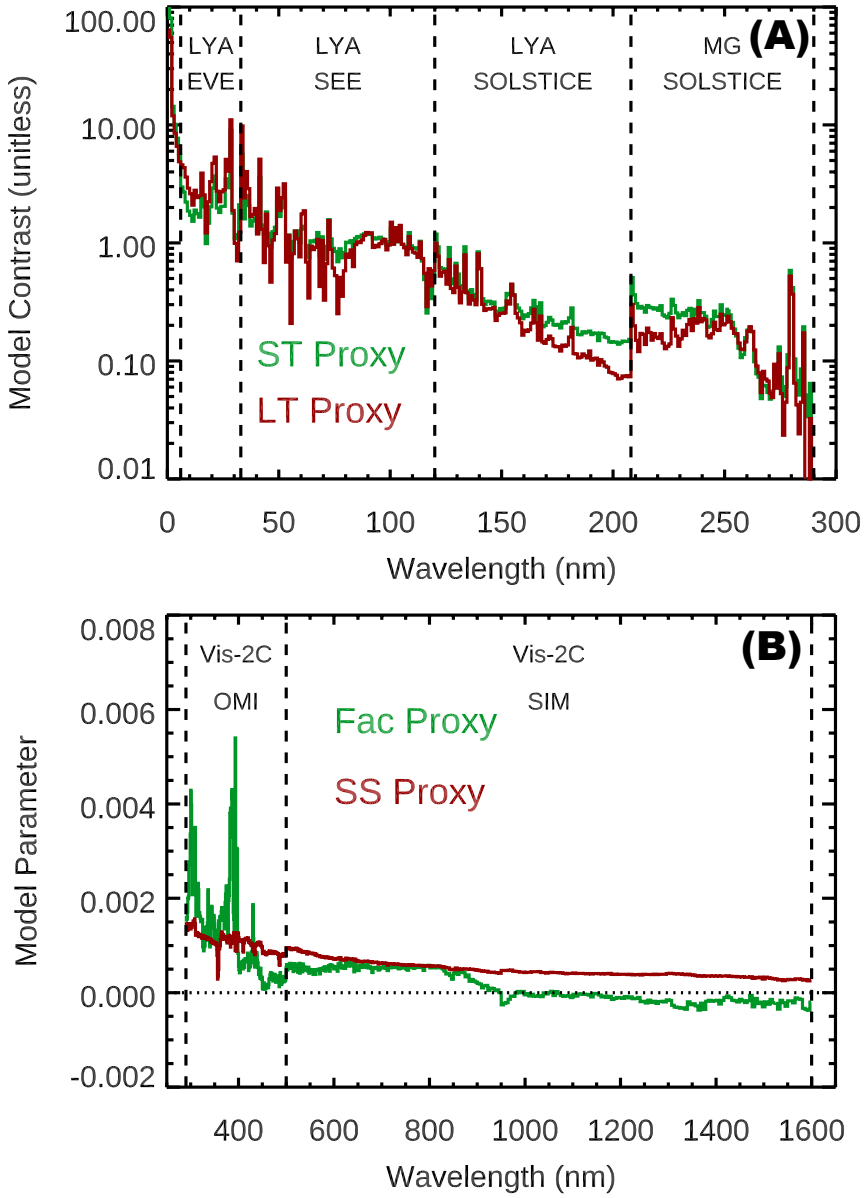

Figure 5. The proxy model parameter values are shown for the single proxy model method (Eq. 1) in panel A and for the two-component (2C) proxy model method (Eq. 2) in panel B. The vertical dashed lines separate where either a different proxy is utilized or a different data set is used. For the 0-6 nm region in panel A, the SORCE XPS data were used with the F10 proxy. The wavelengths with out-of-phase variability are those with the faculae (Fac) proxy values below zero.

774

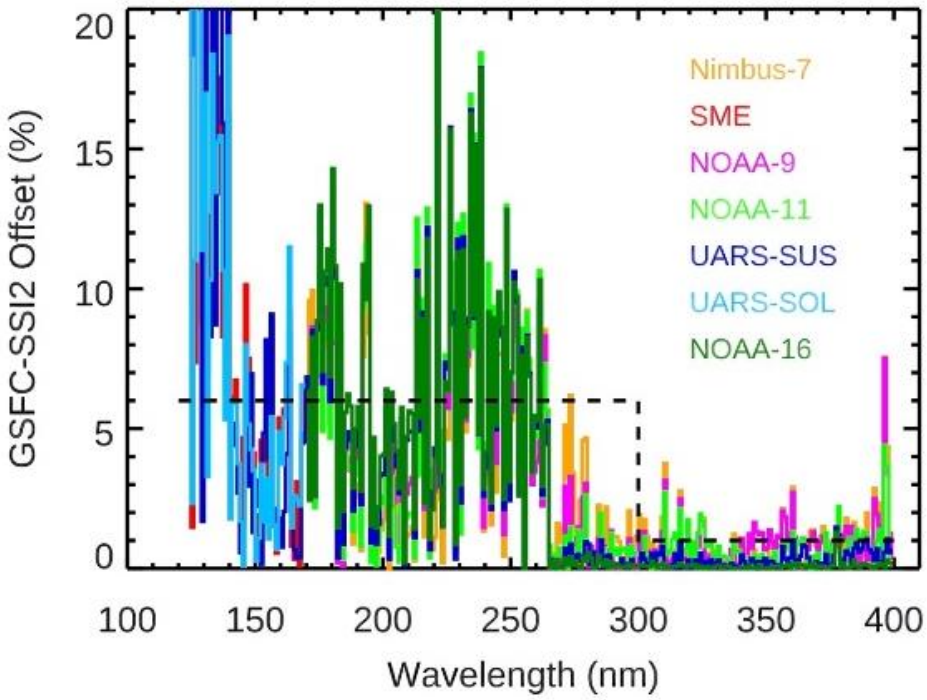

775

776 **Figure 6**. The average offsets for each instrument set in the GSFCSSI2 composite are
777 determined relative to the new SORCE and TSIS-1 reference irradiance levels. The estimated 3-
778 sigma uncertainties for the new reference levels are shown as the dashed lines.

779

780

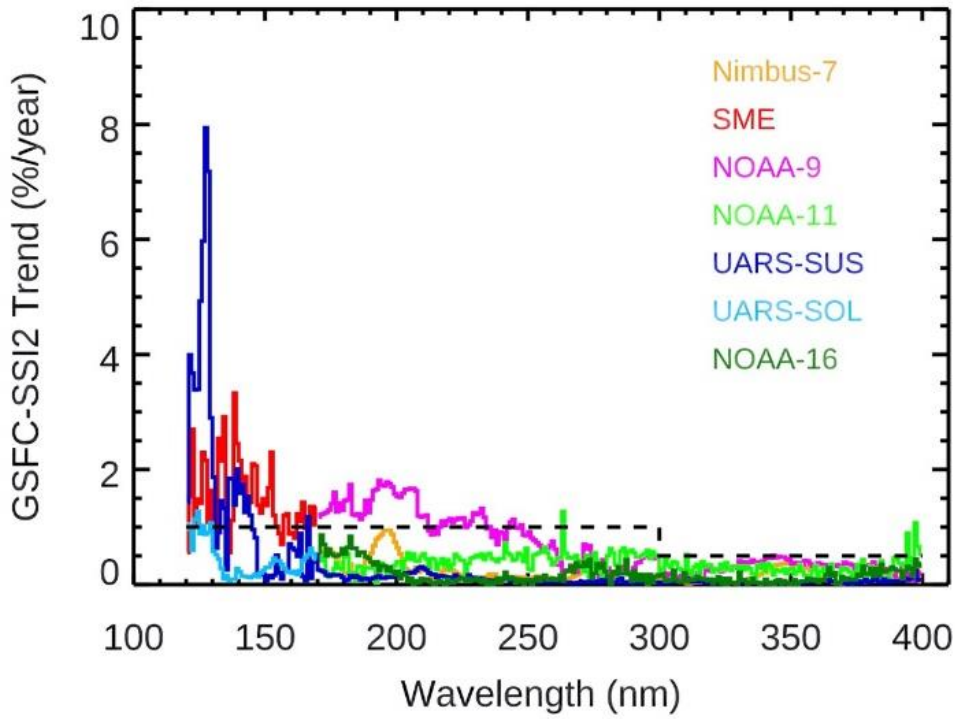

Figure 7. The average long-term trends for each instrument set in the GSFCSSI2 composite are determined relative to the proxy model trends. The estimated trend uncertainties for the new reference sets (SORCE SOLSTICE and OMI) are shown as the dashed lines.

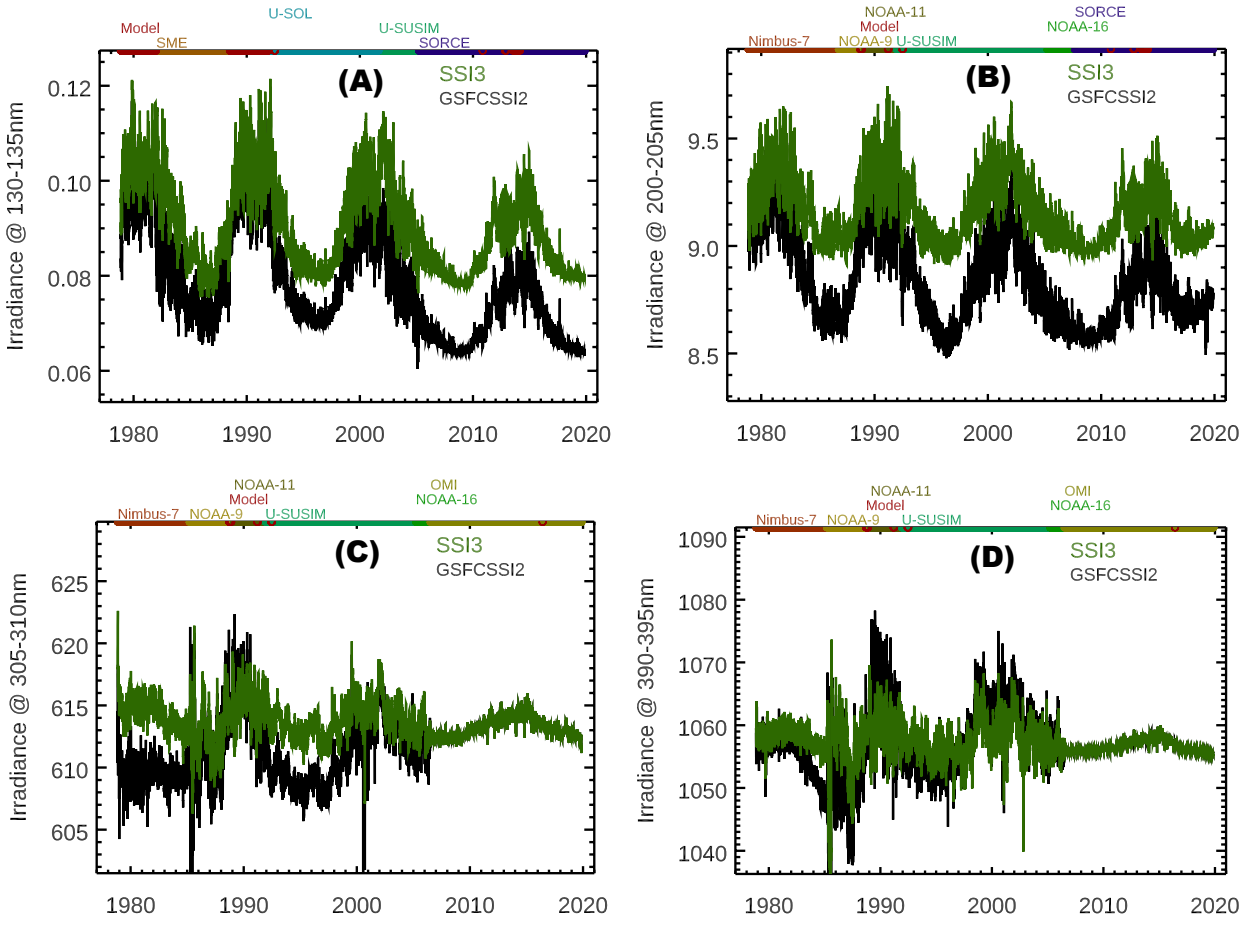

Figure 8. Examples of SSI3 time series are shown for 5-nm bands centered at 132.5 nm (panel A), 202.5 nm (panel B), 307.5 nm (panel C), and 392.5 nm (panel D). The data from the original GSFCSSI2 time series are also shown as the black line, and the sources for those data are shown on the top timeline. The complete description of GSFCSSI2 data selection for each spectral and temporal interval is provided in DeLand et al. (2019).

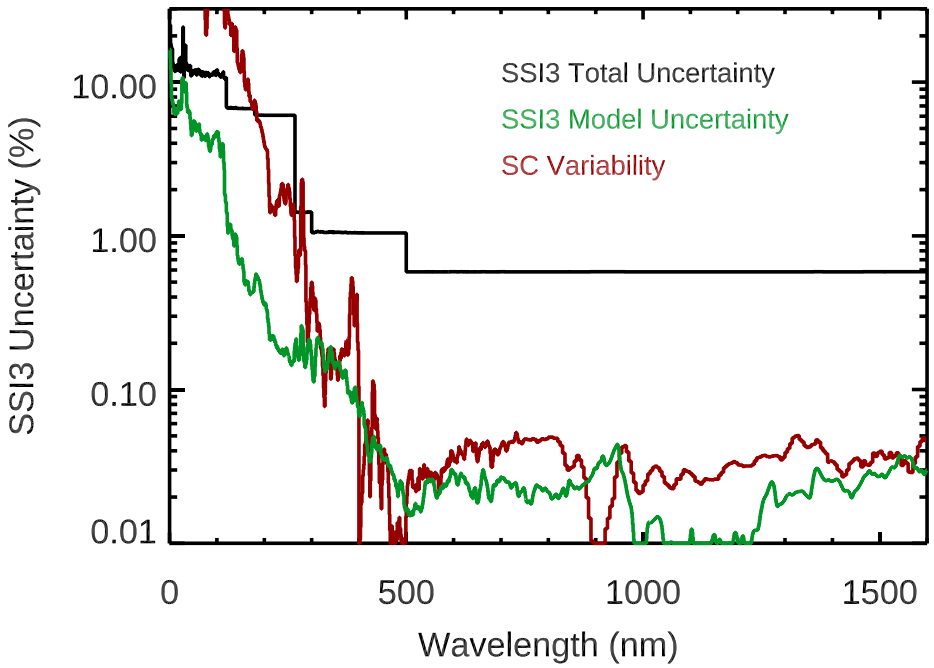

Figure 9. The SSI3 composite total uncertainty (black line) is estimated with the reference data uncertainties, proxy uncertainties, and model fit uncertainties. The model fit uncertainty (green line) can represent a long-term stability estimate for the SSI3 composite. The solar cycle variability (discussed in Section 2) averaged for solar cycles 21-24 is also included as the red line.

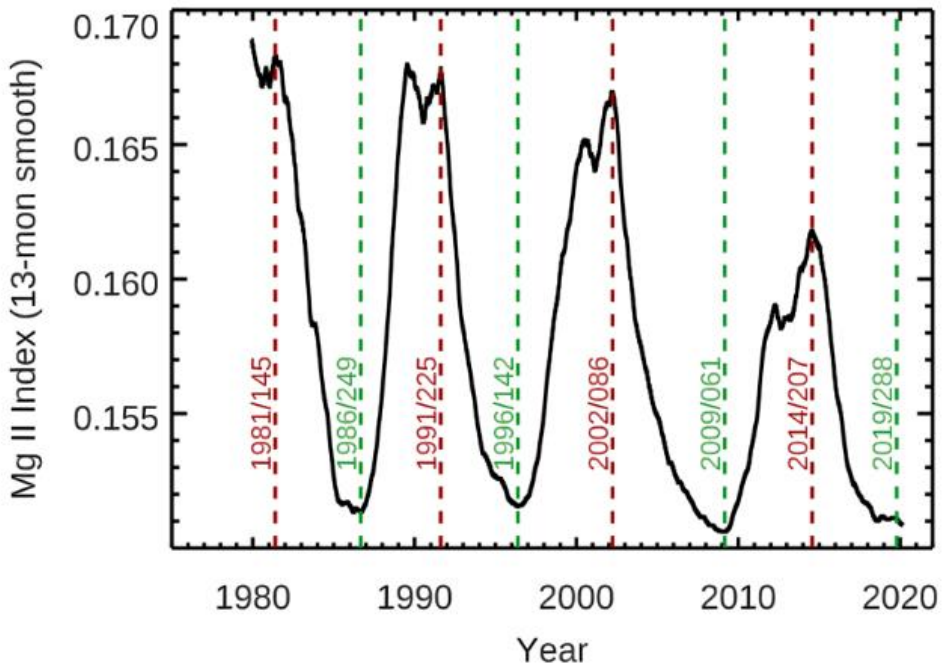

Figure 10. The Mg II index with a 405-day (13-month) smooth is used to identify the solar cycle minimum (green) and maximum (red) dates. This time series starts near the maximum of solar cycle 21 (SC-21) and goes to the end of solar cycle 24 (SC-24). It is interesting to note that the Mg II index has much lower cycle variability for SC-24 than the other solar cycles.

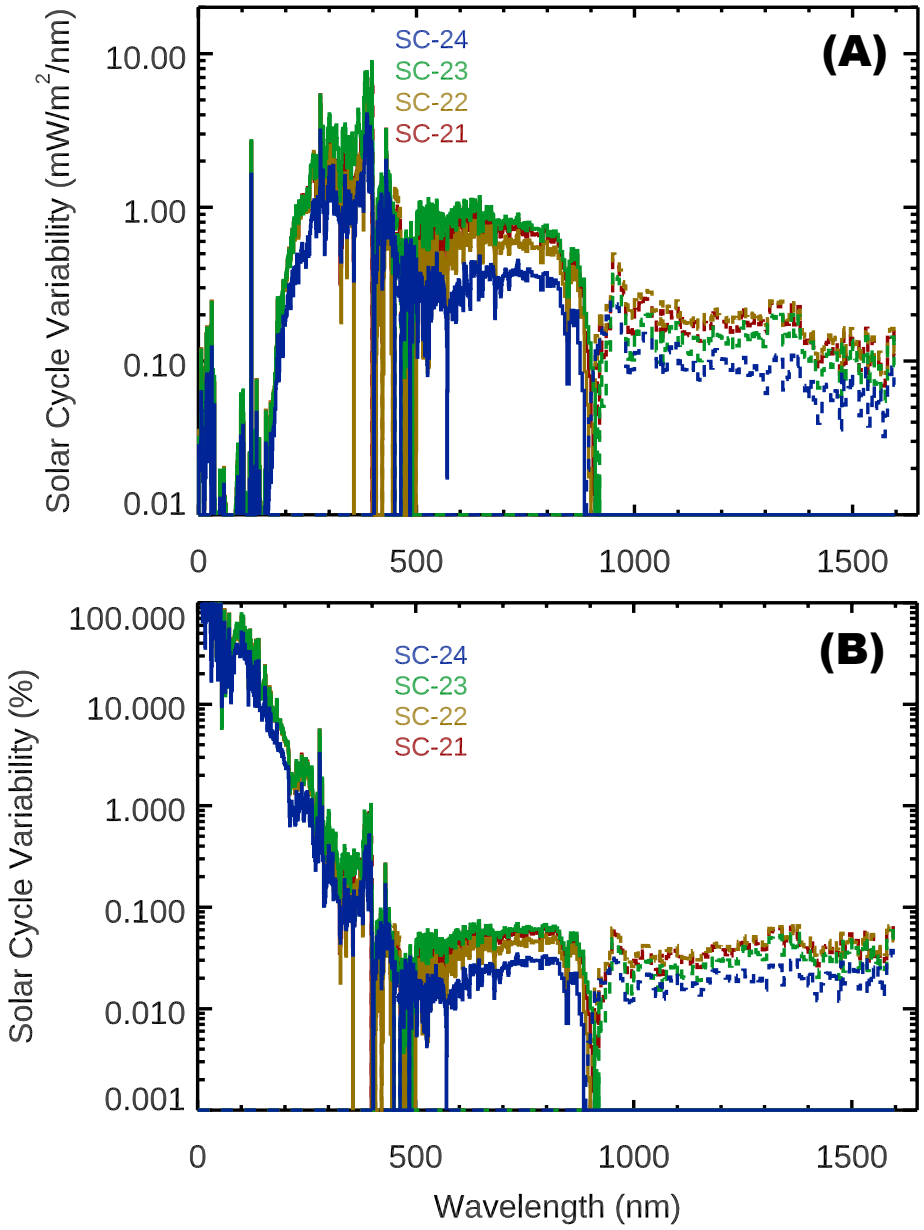

Figure 11. The spectral dependence of solar cycle variability results for the SSI3 composite are shown for four solar cycles. The dates for cycle maximum are those shown in Figure 10, and the minimum is the 2009 minimum. Panel A shows variability in irradiance units (maximum – minimum), and Panel B shows relative variability in percentage change from the 2009 minimum level. Dashed lines indicate out-of-phase (negative) variability, which dominates at wavelengths longer than 900 nm.

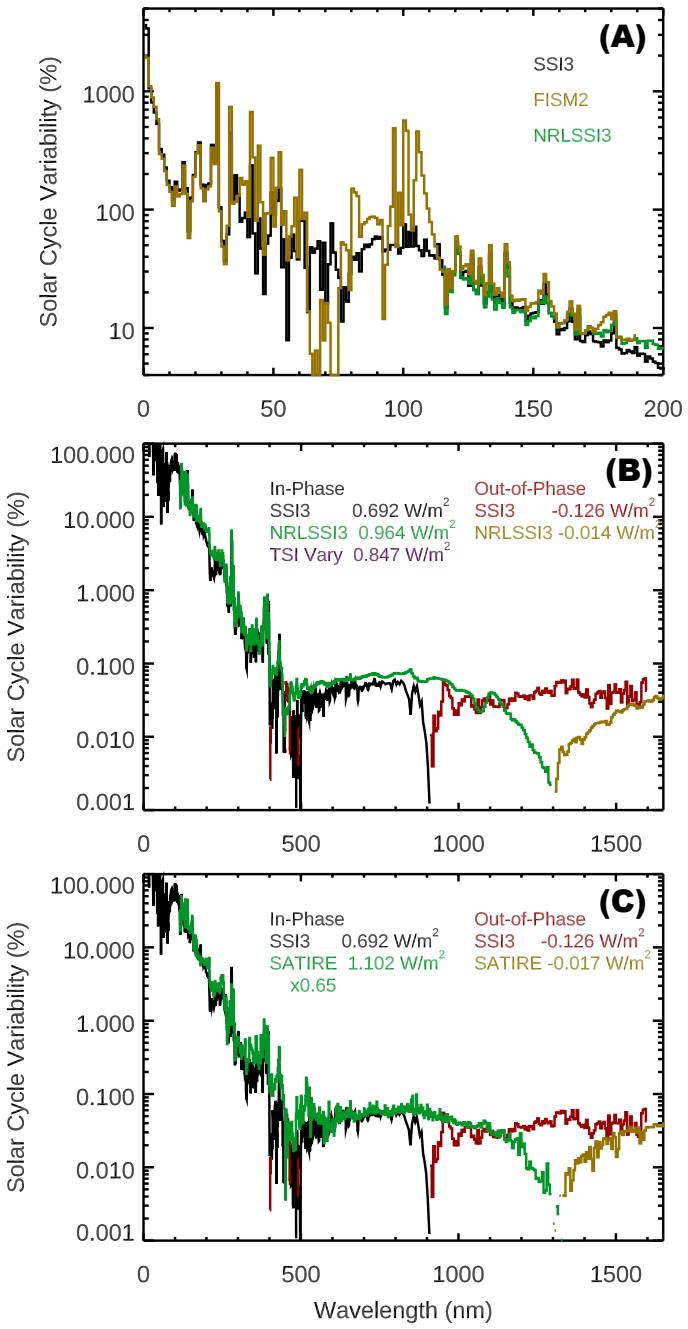

Figure 12. The SSI3 composite solar cycle variability results averaged over four solar cycles are compared to the FISM2 model for FUV and EUV wavelengths (panel A), and to the NRLSSI3 model (panel B) and the SATIRE model (panel C) for the full SSI3 spectral range. The SATIRE model estimate is scaled by 0.5 to match the SSI3 result in the FUV range because the SATIRE estimate only uses 27-day smoothing, instead of the 405-day smoothing used for the SSI3, FISM2, and NRLSSI3 estimates. In panels B and C, the in-phase (positive) variability is shown as the black and green lines, and the out-of-phase (negative) variability is shown as the red and gold lines. The variability numbers in panels B and C are for integration over 0-1600 nm for the SSI3 composite, for integration over 120-1600 nm for NRLSSI3 and SATIRE, and the average of the "TSI Adjust 0-1600 nm" values in Table 3.